

ROLES OF PREPARATION CONDITIONS IN THE MORPHOLOGICAL EVOLUTION OF ELECTRODEPOSITED COPPER

L.H. LIU^{a,b*}, J. LYU^{a,b}, T.K. ZHAO^a, T.H. LI^a

^a*School of Materials Science and Engineering, Northwestern Polytechnical University, Xi'an 710072, PR China;*

^b*Department of Chemical Engineering, University of Michigan, Ann Arbor, Michigan 48109, United States.*

We scrutinized the roles of fabrication conditions in the morphological construction of electrodeposited Cu using generated H₂ bubbles as dynamic negative templates. Adjusting the concentration of acetic acid changed the shapes of the deposited Cu particles, adding cetyltrimethylammonium bromide made the generated Cu easily deposit and grow on the stabilized bubbles for more formation of interconnected dendrites, and decreasing Cu²⁺ concentration resulted in rugged dendritic morphologies. Increasing potential/current densities facilitated the deposition of Cu within the interstitial spaces of smaller bubbles and led to the more formation of interlocked dendrites with smaller pores and Cu particles, while increasing deposition time increased the deposited Cu amount for more dendrites with longer trunks but unvaried branches and Cu particles in size. Based on these investigations, we facilely prepared three-dimensionally bi-continuous porous Cu films under an optimized electrodeposition condition. The films composed of ~300 nm interconnected particles had ~5 μm underneath pores and ~50 μm surface pores with ~10 μm pore wall thickness. Our research paves an avenue for easily fabricating porous metals by considering the effects of the preparation conditions on the morphological evolution of the deposited metals and optimizing the preparation conditions.

(Received June 1, 2017; Accepted October 16, 2017)

Keywords: Porous film; Copper ion; Electrodeposition; Additive type; Electrical field

1. Introduction

Porous metal materials or metallic foams with abundant pores have attracted enormous attention, because of their beneficial characteristics different from their solid counterparts, such as low density, high surface area and high strength and stiffness [1-4]. Especially, porous copper (Cu) materials show comprehensive advantages of low cost, corrosion resistance, high electrical and thermal conductivities, etc, and thus have attracted more attention in various fields of catalyst carriers, electrodes for batteries, separation systems and sensors [5-7].

Traditional fabrication routes like casting and powder metallurgy for porous Cu materials are restrained by high energy depletion related to the high temperature of 800–1300 °C and much processing time [2, 7-12]. Besides, the resulting porous Cu materials exhibit low porosity of <80% and large pore size of hundreds of microns, which are adverse to increasing the surface area and facilitating mass transport as required for the use in the catalytic and electrochemical devices [13-17]. Chemical dealloying is an important template-free method for preparing three-dimensionally (3D) porous Cu materials with high porosity and small pore size even down to several hundred nanometers, but its wide application is severely hindered by the high pollution caused by the excessive use of hazardous acids or bases and inevitable contamination with other compositions [18-21].

The most popular approach for preparing porous materials with controlled morphological features is the sacrificial template-directed method [22-24]. This route includes two main processes: (1) the deposition and growth of new materials in the interstitial spaces of the templates and (2) the

*Corresponding author: liulehao@yahoo.com

removal of the templates by etching or combustion for porous materials. Several kind of hard templates have been usually utilized for the formation of porous materials, such as anodic alumina, polycarbonate and silica [25-27]. It should be mentioned that Liu et al. prepared porous metals by electrodeposition using the generated hydrogen (H_2) gas bubbles arising from the electrochemical reduction of H^+ ions as dynamic negative templates (i.e., the generated metals reduced from metal ions deposited and grew within the interstitial spaces between the H_2 bubble templates to form porous metals) [28-30]. This process has a few merits of low cost, simple preparation, low energy consumption, little processing time and low environmental pollution, compared with the abovementioned methods [1, 31-32]. This method can also afford preparing 3D porous Cu films with small pore size down to several ten microns, high porosity of 80–99%, and thin thickness down to tens of microns [17, 22, 29, 33], though subsequent annealing treatment are sometimes required to improve the mechanical strength of the porous Cu materials [34-36].

Inspired by the discovery by Liu et. al., a few researchers further developed the electrodeposition technique to fabricate porous Cu or alloy films particularly for electrochemical applications [15, 37-43], and studied the effects of additives [1, 3, 22, 29, 44], current density [22] or overpotential [45], deposition time [5, 28, 32], Cu^{2+} ion concentration [46] and electrode composition [47] on the porous Cu films (i.e., the change of the size and distribution of the pores, the dendrite morphology, and the film thickness). However, little attention has been paid to how the preparation conditions affect the morphology of the deposited Cu during the electrodeposition process especially before the formation of the porous Cu films. Thus, it is still interesting to disclose the roles of the preparation conditions in the construction of the electrodeposited Cu materials.

In this study, we fabricated porous Cu materials by electrodeposition using H_2 bubbles as dynamic negative templates (Fig. 1), and investigated the effects of the fabrication conditions (i.e., concentrations of additives and Cu^{2+} ion, applied potential/current densities and deposition time) on the morphological evolution of the deposited Cu. Furthermore, we facilely prepared 3D bi-continuous porous Cu films under an optimized condition. Our work could guide the researchers in theory for easy fabrication of porous metal materials by taking account of the influences of the electrodeposition conditions on the morphological change.

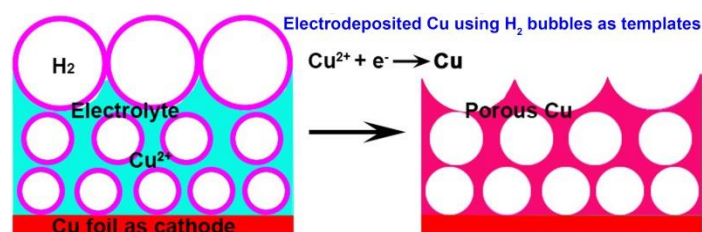


Fig. 1 Schematic presentation of the preparation of porous Cu materials by electrodeposition using generated hydrogen bubbles as dynamic negative templates

2. Experimental details

Prior to the fabrication of porous Cu materials, Cu foils were cleaned with dilute HCl solution (7.4 wt%), acetone, and deionized water, respectively. Porous Cu materials were prepared by utilizing an Epsilon electrochemical workstation (Bioanalytical Systems, Inc.) using two parallel Cu foils as anode and cathode with a distance of ~ 1.5 cm, respectively. A typical electrolyte was a mixture of 0.05 M $CuSO_4$, 1.5 M H_2SO_4 , 0.2 M acetic acid (CH_3COOH), and 2 mM cetyltrimethylammonium bromide (CTAB) solution. For electrochemical deposition of Cu on the cathode, a chronoamperometry (CA) technology was applied under various potentials and time. After the deposition process, the samples were carefully washed with ethanol and deionized water sequentially, and then were dried in a vacuum oven at 60 °C for 12 hours before characterizations. The micromorphology of the electrodeposited Cu materials was investigated by a FEI Nova 200 scanning electron microscope (SEM).

3. Results and discussion

Previous studies have revealed that the addition of acetic acid in the electrolyte can effectively suppress the coalescence of H_2 bubbles and thereby reduce the pore size and increase the pore density of the electrodeposited porous Cu films [29-30]. Here, we investigated the effects of acetic acid on the morphology of the electrodeposited Cu in detail by SEM. Without the addition of acetic acid, quasi-globular Cu particles with a size range of 300–500 nm were deposited on the cathode surface, and a part of the Cu particles interconnected to form agglomerates/aggregates (Fig. 2A-B). When the concentration of acetic acid was 0.1 M, most Cu particles remained irregularly spherical, but some particles changed to be ellipsoidal (Fig. 2C-D). When increasing the acetic acid concentration to 0.2 M, the deposited Cu particles became cubic with an average size of ~ 100 nm, and a few of the Cu nanocubes interlocked to form dendrites (Fig. 2E-F). With the increase of the concentration of acetic acid to 0.3 M, the Cu particles evolved to octahedrons with a size distribution of 60–1100 nm (Fig. 2G-H). Moreover, the octahedral particles interconnected to generate micro-sized agglomerates that further interconnected to create a porous structure. In short, the morphological evolution of the deposited Cu manifests that the increase of the acetic acid concentration can not only reduce the hydrophobic effect of the H_2 bubbles to influence the overall micromorphology of the deposited Cu, but also promote the growth of some certain crystal facets (e.g., $\{100\}$ and $\{332\}$) for the Cu particles with special shapes due to the minimization of the surface free energy.

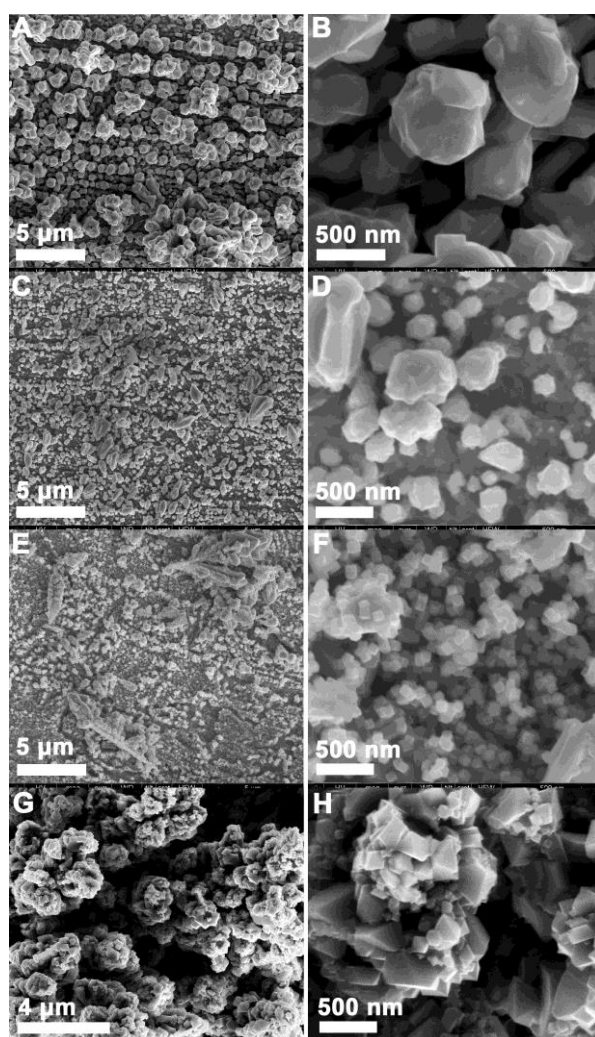


Fig. 2. SEM images of electrodeposited Cu at 30 mV/90 mA cm⁻² for 60 seconds with 0.2 M CuSO₄, 1.5 M H₂SO₄, and (A-B) 0, (C-D) 0.1, (E-F) 0.2 and (G-H) 0.3 M CH₃COOH solutions, respectively.

During the electrodeposition process, the generated H_2 on the electrode surface would coalesce into bigger bubbles and then quickly get away from the electrode. As an important cationic surfactant, CTAB plays important roles in reducing the surface tension of the H_2 bubbles by adhering on the bubble surface and stabilizing the gas bubbles [22, 24]. But excessive CTAB in the electrolyte would lead to the formation of micelles that have no effect on the morphology of the deposited Cu. Without the addition of CTAB in the electrolyte, the generated H_2 bubbles quickly disappeared. As a result, the deposited Cu formed ~ 100 nm particles and only a number of dendrites of tens of microns in length generated because of the interconnection of the nanoparticles (Fig. 3A-B). On the contrary, with the addition of CTAB into the plating solution, the reduced Cu crystal from Cu^{2+} ions easily deposited and grew on the relatively stable H_2 bubbles stabilized by CTAB, and therefore resulted in the formation of interconnected dendrites comprised of ~ 100 nm Cu particles (Fig. 3C-D).

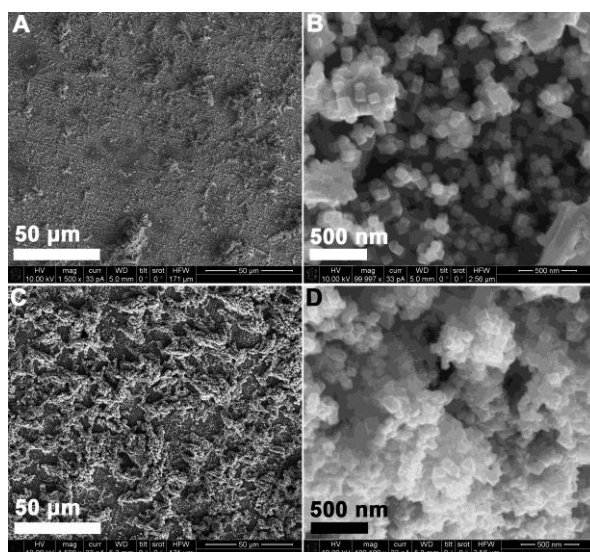


Fig. 3. SEM images of electrodeposited Cu at 30 mV/90 mA cm⁻² for 60 seconds with 0.2 M CuSO₄, 1.5 M H₂SO₄, 0.2 M CH₃COOH, and (A-B) 0 and (C-D) 2 mM CTAB solutions, respectively.

In addition to the additives, the applied potential/current densities had important effects on the morphology of the deposited Cu by increasing the generation rates of Cu and H_2 . When the potential/current densities were 30 mV/90 mA cm⁻², the interlocked dendritic structures composed of ~ 100 nm Cu particles formed with partial coverage on the electrode surface (Fig. 4A-B). When increasing the potential/current densities to 50 mV/150 mA cm⁻², more Cu dendrites generated and interconnected to form a porous network structure with an average pore size of ~ 10 μm (Fig. 4C). Because more H_2 bubbles also generated on the fresh Cu surface, many nanopores formed inside the dendrites constituted with ~ 65 nm Cu particles (Fig. 4D). When increasing the potential/current densities to 200 mV/600 mA cm⁻², more H_2 generated to force the bubbles to get away from the electrode surface and made the bubbles become smaller. Meanwhile, the generation rate of Cu crystal increased to facilitate the deposition of Cu in the interstitial spaces of the smaller H_2 bubbles, and thus the average sizes of the pores of the porous Cu film and the Cu particles decreased to 3 μm and 50 nm, respectively (Fig. 4E-F).

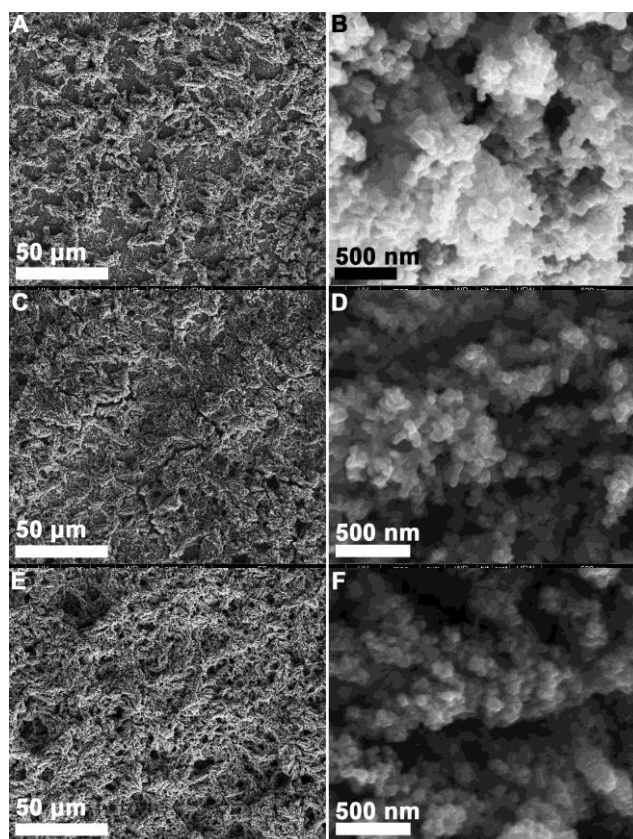


Fig. 4 SEM images of electrodeposited Cu at (A-B) 30/90, (C-D) 50/150, and (E-F) 200/600 mV/mA cm⁻² for 60 seconds with 0.2 M CuSO₄, 1.5 M H₂SO₄, 0.2 M CH₃COOH and 2 mM CTAB solution, respectively.

Deposition time also has important influences on the morphology of the deposited Cu. When being deposited at 30 mV/90 mA cm⁻² for 60 seconds, the generated Cu formed interconnected agglomerates with partial coverage on the electrode surface (Fig. 5A-B). After 120 seconds, the generated Cu crystals completely covered on the electrode surface and formed a 3D porous dendritic structure with average lengths of the trunks and branches of 4.0 μm and 300 nm, respectively (Fig. 5C-D). This was ascribed to the more generation and interconnection of Cu particles to form linear trunks, which further served as fresh electrodes for the generation of Cu and H₂ and therefore caused the formation of new branches. Moreover, the average size of the Cu particles was 60 nm. After 180 seconds of deposition, the average length of the trunks increased to 4.5 μm (Fig. 5E-F). However, the average sizes of the branches and the Cu particles remained unchanged, because of the unvaried generation rates of Cu and H₂ under the same potential/current densities. These findings revealed that the trunks had a higher growth rate than the branches, which was attributed to the large size, high reaction area and enhanced electrical contact of the trunks and the resulted preferential deposition and growth of Cu on the trunks.

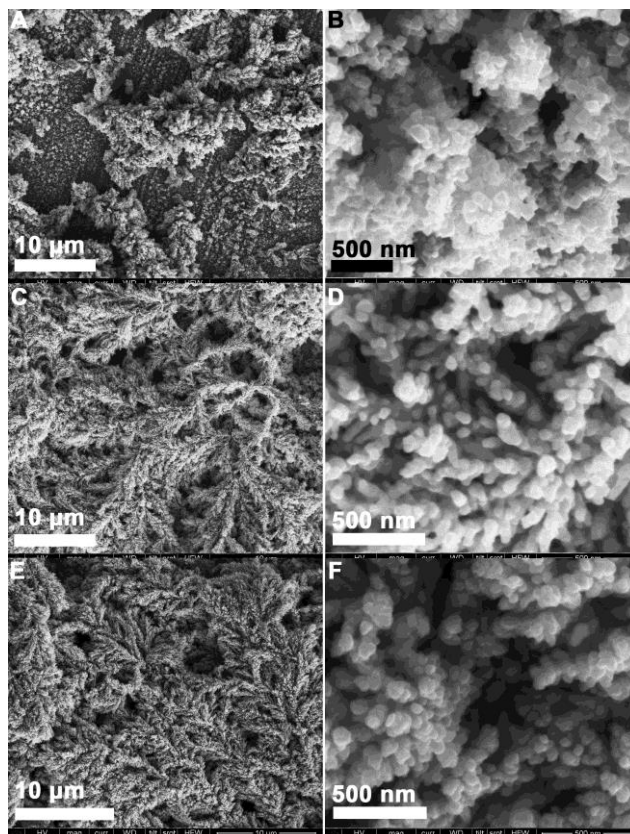


Fig. 5. SEM images of electrodeposited Cu at 30 mV/90 mA cm⁻² for (A-B) 60, (C-D) 120, and (E-F) 180 seconds with 0.2 M CuSO₄, 1.5 M H₂SO₄, 0.2 M CH₃COOH and 2 mM CTAB solution, respectively.

Cu and H₂ simultaneously and competitively generated on the cathode surface closely related to the reduction reactions of Cu²⁺ and H⁺ ions during the electrodeposition process. Therefore, varying the concentration of Cu²⁺ would influence the generation rates of Cu and H₂, and further affect the morphology of the deposited Cu. When being electrodeposited under 800 mV/2.4 A cm⁻² for 60 seconds using 0.2 M CuSO₄ solution, a 3D porous Cu film with a relatively flat surface entirely covered on the electrode surface, and the average sizes of the pores formed by the dendrites and the essential building units—Cu particles were 2.5 μm and 60 nm, respectively (Fig. 6A-C). Such small dimensional characteristics have not been observed in the reported electrodeposited Cu films probably due to the improper fabrication conditions, and are comparable to those of the porous Cu films obtained by dealloying [18, 48-50] and our reported nanoparticle assembly routes [17]. When decreasing the Cu²⁺ concentration to 0.1 M, the porous Cu film with micro-sized pores almost fully covered on the whole electrode surface (Fig. 6D-F). When decreasing the Cu²⁺ concentration to 0.05 M, the porous dendritic structure cannot completely cover on the electrode surface, but formed a rugged terrain, which was constituted with many valleys owing to the less deposited Cu (Fig. 6G-I). This phenomenon can be explained as follows: with the decrease of the Cu²⁺ concentration, more H₂ generated and coalesced into bigger bubbles because of the competitive generation of Cu and H₂ [22], but less Cu generated and grew slowly in the interstitial spaces between the bubbles, thus resulting in the relatively rugged morphology.

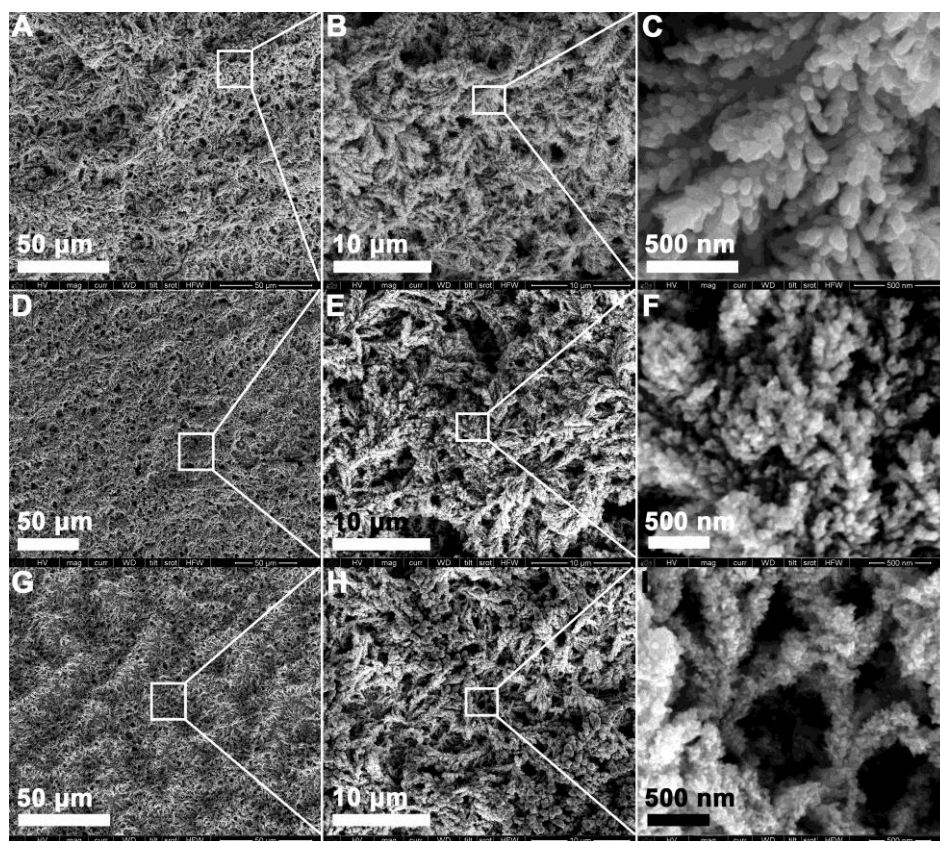


Fig. 6. SEM images of electrodeposited Cu at 800 mV/2.4 A cm⁻² for 60 seconds with 1.5 M H₂SO₄, 0.2 M CH₃COOH and 2 mM CTAB, and (A-C) 0.2, (D-F) 0.1 and (G-I) 0.05 M CuSO₄ solutions, respectively.

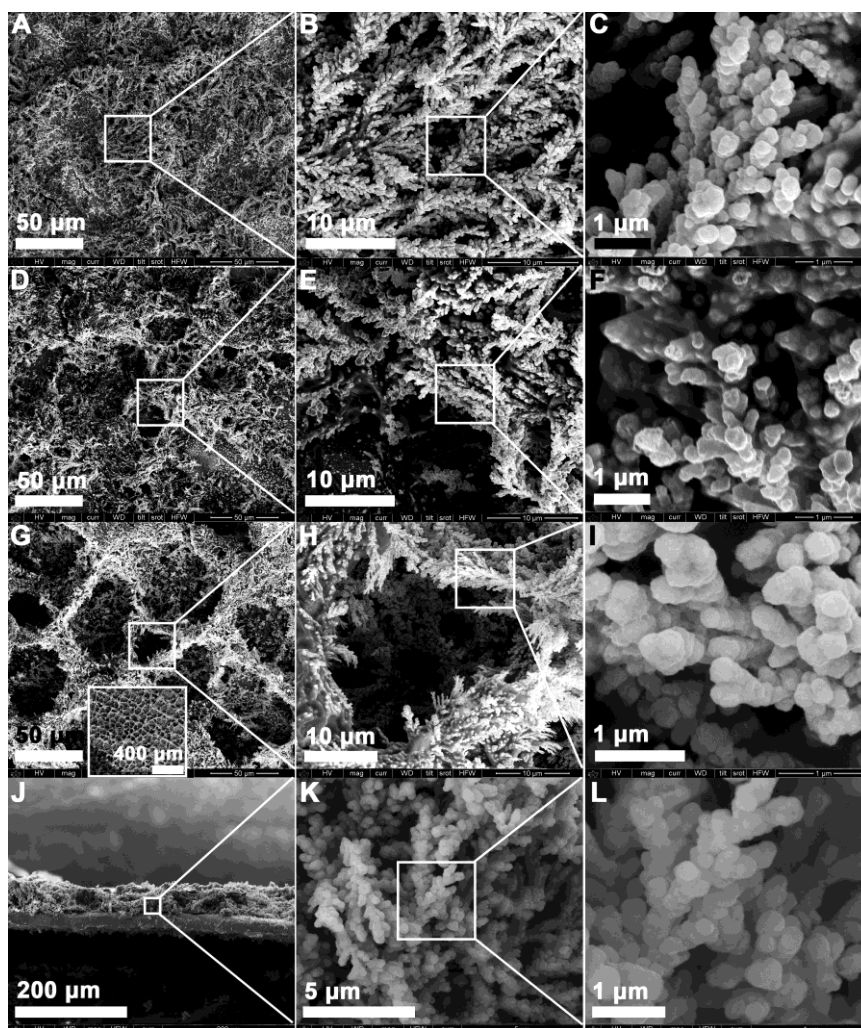


Fig. 7 SEM images of electrodeposited Cu at $800\text{ mV}/2.4\text{ A cm}^{-2}$ for (A-C) 120, (D-F) 180, and (G-I) 240 seconds with 0.05 M CuSO_4 , $1.5\text{ M H}_2\text{SO}_4$, $0.2\text{ M CH}_3\text{COOH}$ and 2 mM CTAB solution, respectively. The inset in (G) is a lower-magnification SEM image corresponded to (G). (J-L) show the corresponding cross-sectional images of (G-I).

Bearing the aforesaid investigations on the electrodeposition conditions in mind, we decided to fabricate 3D bi-continuous porous Cu films under an optimized condition. When being electrodeposited under $800\text{ mV}/2.4\text{ A cm}^{-2}$ for 120 seconds, the deposited Cu formed a porous dendritic structure with partial coverage on the electrode surface (Fig. 7A-C). After 180 seconds, the dendrites continued to grow and interconnected to form pores of tens of microns (Fig. 7D-F). However, the dendritic structure still could not completely cover on the electrode surface, because of the small amount of deposited Cu in the limited time. After 240 seconds, more dendrites grew and interlocked to create a 3D porous Cu film with an average pore size of $50\text{ }\mu\text{m}$ and an average thickness of the pore walls of $10\text{ }\mu\text{m}$ (Fig. 7G), which agreed with the previous reports [1, 22, 28-29, 47]. Higher-resolution SEM further revealed that many $\sim 5\text{ }\mu\text{m}$ pores formed beneath the $\sim 50\text{ }\mu\text{m}$ surface pores (Fig. 7H), indicating a bi-continuous porous configuration. To better explain this phenomenon, it is necessary to disclose the electrodeposition process in detail. During the process, the generated H_2 first formed small bubbles on the cathode surface, and the generated Cu deposited and grew using the small bubbles as templates to form the porous dendritic structure with small pores; the formerly generated small bubbles got away from the cathode surface due to the repulsive force from the newly generated bubbles and coalesced into bigger bubbles with the assistance of hydrophobic force on the dendritic Cu surface, and the newly generated Cu deposited and grew using the bigger bubbles as templates and thereby resulted in the formation of bigger pores away

from the cathode (i.e., on the top surface of the porous Cu film). The branches of the dendrites were several microns in length, and were also composed of ~ 300 nm Cu particles (Fig. 7I). The thickness of the porous Cu film was determined to be ~ 55 μm (Fig. 7J). Even inside the cross-section of the film, the Cu particle-assembled dendrites still retained the loosen construction (Fig. 7K-L), which was well consistent with the surface morphology (Fig. 7H-I).

4. Conclusions

We scrutinized the roles of the fabrication conditions in the morphological construction of the electrodeposited Cu using the generated H_2 bubbles as dynamic negative templates: (1) the addition of acetic acid in the plating bath can not only reduce the hydrophobic force of the H_2 bubbles to affect the micromorphology of the deposited Cu, but also promote the growth of some crystal facets (e.g., $\{100\}$ and $\{332\}$) for the Cu particles with special shapes due to the minimization of the surface free energy; (2) the addition of CTAB could stabilize the H_2 bubbles by reducing their surface tension and make the generated Cu easily deposit and grow on the relatively stable H_2 bubbles for more formation of interconnected dendrites; (3) decreasing the Cu^{2+} ion concentration would result in the relatively rugged dendritic morphology caused by the competitive generation of Cu and H_2 ; (4) increasing the potential/current densities facilitated the deposition of Cu within the interstitial spaces of smaller H_2 bubbles and therefore led to the formation of more interlocked dendritic structures with smaller pores and Cu particles; (5) increasing the deposition time increased the deposition mass of Cu for more dendrites with longer trunks but unvaried branches and Cu particles in size. Based on these investigations, we facilely prepared 3D bi-continuous porous Cu films under an optimized electrodeposition condition. Specifically, the porous Cu films composed of ~ 300 nm interconnected Cu particles had ~ 5 μm underneath pores and ~ 50 μm surface pores with ~ 10 μm pore wall thickness. We hope our study on the effects of the preparation conditions on the morphological change of the electrodeposited Cu could guide the researchers in theory for easily fabricating porous metal materials by optimizing the electrodeposition conditions.

Acknowledgments

This work was partly supported by China Aeronautical Science Fund (2014ZF53074), the Innovation Fund of China Aerospace Science and Technology (CASC200906), the Supporting Program of China Aerospace Science and Technology (CASC201209), the Specialized Research Fund for the Doctoral Program of Higher Education (20096102120016), the National Natural Science Foundation of Shaanxi (2009GM6001-1), the Key Science and Technology Program of Shaanxi (2013K09-03), and the National Natural Science Foundation of China (51172184).

References

- [1] D. Nam, R. Kim, D. Han, J. Kim, H. Kwon, *Electrochim. Acta* **56**, 9397 (2011).
- [2] J. Park, S. Hyun, S. Suzuki, H. Nakajima, *Acta Mater.* **55**, 5646 (2007).
- [3] N. Wang, W. C. Hu, Y. H. Lu, Y. F. Deng, X. B. Wan, Y. W. Zhang, K. Du, L. Zhang, *Trans. IMF* **89**, 261 (2011).
- [4] M. Sabzevari, S. A. Sajjadi, A. Moloodi, *Adv. Powder Technol.* **27**, 105 (2016).
- [5] N. D. Nikolić, G. Branković, K. I. Popov, *Mater. Chem. Phys.* **125**, 587 (2011).
- [6] Y. Zhang, P. Zhu, L. Chen, G. Li, F. Zhou, D. D. Lu, R. Sun, F. Zhou, C.-P. Wong, *J. Mater. Chem. A* **2**, 11966 (2014).
- [7] J. Ru, B. Kong, Y. Liu, X. Wang, T. Fan, D. Zhang, *Mater. Lett.* **139**, 318 (2015).
- [8] Y. Ahmed, M. Riad, A. Sayed, M. Ahlam, M. Shalabi, *Powder Technol.* **175**, 48 (2007).
- [9] Y. Zhao, T. Fung, L. Zhang, F. Zhang, *Scripta Mater.* **52**, 295 (2005).

- [10] S. Hyun, K. Murakami, H. Nakajima, *Mater. Sci. Eng. A* **299**, 241 (2001).
- [11] S. Hyun, H. Nakajima, *Mater. Lett.* **57**, 3149 (2003).
- [12] S. K. Hyun, H. Nakajima, *Mater. Sci. Eng. A* **340**, 258 (2003).
- [13] W. B. Liu, S. C. Zhang, N. Li, J. W. Zheng, Y. L. Xing, *Micropor. Mesopor. Mater.* **138**, 1 (2011).
- [14] T. Song, M. Yan, Z. Shi, A. Atrens, M. Qian, *Electrochim. Acta* **164**, 288 (2015).
- [15] L.-J. Xue, Y.-F. Xu, L. Huang, F.-S. Ke, Y. He, Y.-X. Wang, G.-Z. Wei, J.-T. Li, S.-G. Sun, *Electrochim. Acta* **56**, 5979 (2011).
- [16] K. T. Lee, J. C. Lytle, N. S. Ergang, S. M. Oh, A. Stein, *Adv. Funct. Mater.* **15**, 547 (2005).
- [17] L. Liu, B. G. Choi, S. O. Tung, T. Hu, Y. Liu, T. Li, T. Zhao, N. A. Kotov, *Faraday Discuss.* **181**, 383 (2015).
- [18] J. Hayes, A. Hodge, J. Biener, A. Hamza, K. Sieradzki, *J. Mater. Res.* **21**, 2611 (2006).
- [19] Z. Dan, F. Qin, A. Makino, Y. Sugawara, I. Muto, N. Hara, *J. Alloy. Compd.* **586**, S134 (2014).
- [20] T. Aburada, J. M. Fitz-Gerald, J. R. Scully, *Corros. Sci.* **53**, 1627 (2011).
- [21] X. Li, B. Huang, C. Qiu, Z. Li, L.-H. Shao, H. Liu, *J. Alloy. Compd.* **681**, 109 (2016).
- [22] Y. Li, W.-Z. Jia, Y.-Y. Song, X.-H. Xia, *Chem. Mater.* **19**, 5758 (2007).
- [23] H. Ji, L. Zhang, M. T. Pettes, H. Li, S. Chen, L. Shi, R. Piner, R. S. Ruoff, *Nano Lett.* **12**, 2446 (2012).
- [24] Y. Li, Y.-Y. Song, C. Yang, X.-H. Xia, *Electrochem. Commun.* **9**, 981 (2007).
- [25] P.-L. Taberna, S. Mitra, P. Poizot, P. Simon, J.-M. Tarascon, *Nat. Mater.* **5**, 567 (2006).
- [26] Y. Guo, H. Yui, H. Minamikawa, B. Yang, M. Masuda, K. Ito, T. Shimizu, *Chem. Mater.* **18**, 1577 (2006).
- [27] F. Dai, J. Zai, R. Yi, M. L. Gordin, H. Sohn, S. Chen, D. Wang, *Nat. Commun.* **5**, 1 (2014).
- [28] H. C. Shin, J. Dong, M. Liu, *Adv. Mater.* **15**, 1610 (2003).
- [29] H.-C. Shin, M. Liu, *Chem. Mater.* **16**, 5460 (2004).
- [30] H.-C. Shin, M. Liu, *Adv. Funct. Mater.* **15**, 582 (2005).
- [31] L. Liu, J. Lyu, T. Zhao, T. Li, *Chem. Eng. Commun.* **203**, 707 (2016).
- [32] H. Wang, N. Wang, T. Hang, M. Li, *Appl. Surf. Sci.* **372**, 7 (2016).
- [33] P. Liu, K. Liang, *J. Mater. Sci.* **36**, 5059 (2001).
- [34] X.-Y. Fan, F.-S. Ke, G.-Z. Wei, L. Huang, S.-G. Sun, *J. Alloy. Compd.* **476**, 70 (2009).
- [35] L. Trahey, J. T. Vaughey, H. H. Kung, M. M. Thackeray, *J. Electrochem. Soc.* **156**, A385 (2009).
- [36] T. Jiang, S. Zhang, X. Qiu, M. Sun, L. Chen, *Electrochem. Solid-St. Lett.* **11**, D50 (2008).
- [37] J. Suk, D. Y. Kim, D. W. Kim, Y. Kang, *J. Mater. Chem. A* **2**, 2478 (2014).
- [38] H. Wu, N. Du, J. Wang, H. Zhang, D. Yang, *J. Power Sources* **246**, 198 (2014).
- [39] V. D. Patake, S. S. Joshi, C. D. Lokhande, O.-S. Joo, *Mater. Chem. Phys.* **114**, 6 (2009).
- [40] T. Jiang, S. Zhang, X. Qiu, W. Zhu, L. Chen, *J. Power Sources* **166**, 503 (2007).
- [41] D. H. Nam, R. H. Kim, D. W. Han, H. S. Kwon, *Electrochim. Acta* **66**, 126 (2012).
- [42] L. Liu, J. Lyu, T. Li, T. Zhao, *Nanoscale* **8**, 701 (2016).
- [43] L. Liu, F. Xie, J. Lyu, T. Zhao, T. Li, B. G. Choi, *J. Power Sources* **321**, 11 (2016).
- [44] J.-H. Kim, R.-H. Kim, H.-S. Kwon, *Electrochem. Commun.* **10**, 1148 (2008).
- [45] N. D. Nikolić, K. I. Popov, L. J. Pavlović, M. G. Pavlović, *J. Electroanal. Chem.* **588**, 88 (2006).
- [46] N. D. Nikolic, K. I. Popov, L. J. Pavlovic, M. G. Pavlovic, *Sensors* **7**, 1 (2007).
- [47] I. Najdovski, A. P. O'Mullane, *J. Electroanal. Chem.* **722**, 95 (2014).
- [48] Z. Qi, C. Zhao, X. Wang, J. Lin, W. Shao, Z. Zhang, X. Bian, *J. Phys. Chem. C* **113**, 6694 (2009).
- [49] L.-Y. Chen, J.-S. Yu, T. Fujita, M.-W. Chen, *Adv. Funct. Mater.* **19**, 1221 (2009).
- [50] H. Jo, Y.-H. Cho, M. Choi, J. Cho, J. H. Um, Y.-E. Sung, H. Choe, *Mater. Chem. Phys.* **145**, 6 (2014).